Chapter II.3 The Twin-Flow Microrespirometer and Simultaneous Calorimetry

E. Gnaiger[1]

1 Introduction

Continuous long-term monitoring of respiratory rates in aquatic organisms is only possible in open-flow systems providing controlled environmental conditions during the experiment. This is a basic requirement for many topics in ecophysiological and applied research, and there is an apparent need for more detailed respiratory studies with organisms of different size and under a wide range of conditions. The most important aspects are: metabolic adaptation and acclimation to environmental factors (Chap. II.2); functional relations of oxygen uptake and locomotory activity (Chap. II.5) and growth; internal rhythms (Chap. II.7); quantification of respiratory energy loss complementing assimilation and production measurements in energy budget studies (Chap. III.4); sublethal effects of environmental contaminants; biological oxygen demand in water quality control.

Microrespirometers are commonly closed, thus not permitting extended experimental periods without the interference of uncontrolled variables. Methodological difficulties arise since the mere miniaturization of an ordinary respirometry system does not produce a functional microrespirometer. Due to the unfavorable volume-to-surface ratio in animal chambers with a volume less than 0.5 to 1 cm^3, increasing attention has to be paid to problems of oxygen diffusion and bacterial growth. The respiratory rate per unit volume (closed systems) or throughflow (open systems) is likely to decrease with size of the experimental animal, since reduction of volume or of throughflow entails new limitations of system functions. Consequently, an improved sensitivity and stability of the measuring and recording system is required. The twin-flow microrespirometer was developed to meet the need for a new apparatus for automatic and continuous monitoring of oxygen uptake in small aquatic animals. This instrument combines the following features:

a) Long-term stability and high precision. This is achieved by use of two polarographic oxygen sensors (POS) alternately switched to the measuring or the calibration position (twin-flow principle). Thus automatic control of baseline stability is possible without interruption of the oxygen record.

1 Institut für Zoologie, Abteilung Zoophysiologie, Universität Innsbruck, Peter-Mayr-Str. 1A, A–6020 Innsbruck, Austria

Polarographic Oxygen Sensors (ed. by Gnaiger/Forstner)

b) High sensitivity and time resolution. Miniaturization of the stirring chambers and minimal dead volume reduce the response time. A good time resolution of metabolic patterns is achieved even at low rates of throughflow, when the system is run at its lower limit of detection (3 nmol O_2 h^{-1}).

c) Controlled environmental conditions. The open-flow system permits long-term recording of oxygen uptake at constant levels of oxygen concentration. Parameters of the medium can be altered during the experiment (e.g., in toxicological studies) without interfering with the continuous record of respiration.

d) Flexibility. Every type of animal chamber can be used in conjunction with the twin-flow system which therefore can be adapted for several types of aquatic organisms and for the simultaneous monitoring of additional physiological parameters (e.g., locomotory activity).

e) Simultaneous calorimetry. The twin-flow microrespirometer was specifically designed to provide a constant flow regime even during calibration. This is a basic prerequisite for simultaneous respirometry and calorimetry in an open-flow system.

Under aerobic and balanced physiological conditions, excellent agreement between indirect (respirometric) and direct calorimetry was observed over short as well as long periods of time (cf. Chap. II.4). In these situations accurate calculation of respiratory energy dissipation is possible (App. C). Under behavioral, environmental, and toxicological stress, however, total energy dissipation (aerobic and anoxic processes) can be considerably higher than indicated by aerobic respiration. Simultaneous direct and indirect calorimetry not only open new perspectives in ecological bioenergetics, they assist in exploring mechanisms of metabolic energy expenditure.

2 Choice of the Proper Respirometer

At the present stage of technology, the choice for the construction or – if available – for the purchase of a particular type of respirometer is predominantly governed by economic considerations. The biological arguments for or against the various systems have been widely discussed and the technical problems have been solved in principle even for the more extravagant fields of application such as in situ measurements in the deep sea (Chap. III.5) or for space biology [20]. However, the capital investment involved is unrealistic for standard laboratory applications. On the other hand, inexpensive and simple respirometric techniques may result in scientific and economic failure if the hours wasted on unsatisfactory experiments are taken into account. Such costly experience stimulated the perfection of the twin-flow respirometry system for the automatic long-term monitoring of oxygen uptake in very small macrofauna or a reasonable number of meiofauna (< 1 mg dry weight of biomass).

2.1 Gasometric Methods

The most sensitive microrespirometers (10^{-3} to 10^{-5} μmol O_2 h^{-1}) are modifications of the Cartesian diver technique [29, 49] which is becoming increasingly important in

studies of unicellular species and meiofauna (< 0.1 mg wet weight). In the case of the electromagnetic diver [33], recording is automatic and continuous. Its application requires high skill and practice, especially if metabolic effects of low p_{O_2} levels are studied [32]. The water volume in the diver has to be kept small to avoid diffusion errors. When confined in a drop of water zooplankton and other active animals are restricted in their locomotory behavior: some copepod species die within 2 to 10 h in the Cartesian diver [21]. A premortal increase in metabolic rate followed a plateau, the physiological interpretation of which may be complex, although the level of oxygen consumption agreed with that measured in an open-flow system [21].

If the experimental oxygen uptake rates are in the order of 1 μmol O_2 h^{-1}, Warburg and Gilson respirometers may be considered for studies of small aquatic animals. However, a comparison of methods makes evident that shaking the respirometer flask disturbs the animals and influences metabolic rates (Table 1). While the average rate is doubled in aquatic oligochaetes by shaking, it decreases in other animals [48]. Non-wetting species such as *Daphnia* are caught in the surface film of the water in shaken Warburg flasks. Good agreement between oxygen uptake under these highly abnormal conditions with that in a closed bottle respirometer [44] suggests cautious interpretation of results obtained with both of these methods (see below). Since agitation distors the respiratory response to other environmental factors in various species [42], the Warburg method cannot be recommended for monitoring the physiological effect on animals of aquatic pollutants.

In nearly all gasometric respirometers, the gas phase in equilibrium with the medium containing the organism is scrubbed free of carbon dioxide. Although alimination of CO_2 has no detectable effect on *Lumbriculus* [14], it decreases the metabolic rate of other species [45, 48].

2.2 Open Versus Closed Respirometric Systems

Analysis of dissolved oxygen circumvents the problem of CO_2 absorption and p_{O_2} equilibration between the aqueous and gaseous phase. Without much instrumental expense and with some practical skill, the micro-Winkler method (App. D) may be used in a simple closed-bottle respirometric technique. Disturbance of the animals by transfer into a respirometer usually results in greatly increased oxygen uptake rates during the first hours of the experiment [21, 25, 45]. This may explain a large fraction of the difference in rates obtained with the closed-bottle and open-flow respirometric method [8, 25]. The continuous record of oxygen uptake by POS aids substantially in interpreting the results.

Various additional factors acting in concert may obscure the physiological interpretation of measurements made in closed systems: because oxygen is gradually depleted in the course of the experiment, respiration decreases in animals whose respiration rate is oxygen-dependent. At the same time, the rate may be unstable due to starvation. Continuous monitoring by POS of p_{O_2} down to oxygen depletion in closed systems reveals a response to the rapid change in oxygen content [34]. This response may, however, be masked by other effects varying with time in an uncontrolled manner [13]. Due to the fact that in closed respirometers no sustained measurements are

Table 1. Comparison of manometric (Warburg) respirometry involving shaking of the animal chamber (A) and methods without mechanical disturbance of the animals (B–C); B: closed system respirometry with continuous or discontinuous p_{O_2} analysis by Winkler or POS; C: microcalorimetric flow method, the oxygen equivalent of heat production was estimated at 1 mW ≙ 8 μmol O_2 h^{-1} ≙ 0.18 cm^3 O_2 h^{-1} (App. C). Test animals: *Tubifex tubifex* (T.t.) and *Lumbriculus variegatus* (L.v.) (Oligochaeta). Experimental temperatures (θ_{exp}) and individual wet weights ($_wW_{exp}$) are given. Dry weight is 0.17 × $_wW$

Method	Species	θ_{exp} (°C)	$_wW_{exp}$ (mg)	$\dot{n}_{O_2}$ (20°C) μmol O_2 h^{-1} g^{-1} Range[a]	Mean[a]	Mean[b]	Ref.
A	T.t.	18–20	?	9.2–13.8	11.9		[22]
A	T.t	17–19	?	12.9–24.6	18.2		[31]
A	L.v.	20	?	6.2– 9.0	7.6		[28]
A	T.t.	25	1.9	12.7–21.6	16.6	11.0	[11]
A	T.t.	20	2.5	23.4–25.6	24.5	17.4	[40]
A	T.[c]	20(?)	?	11.8–24.6	18.8		[47]
A	L.v.	20	10/1	10.4–18.4[d]	14.4	10.4	[g]
A	T.t.	20	7.8	4.5– 6.3	5.4	5.0	[7]
				9.4–19.9[e]	14.7	11.0	
B	T.t.	19	?	6.7– 7.4	7.1		[g]
B	T.t.	14	6	8.6– 9.5	9.0	7.9	[g]
B	T.t.	20	10/1	4.4– 8.1[d]	6.2	4.4	[g]
B	T.t.	20	2.4	3.2– 4.1	3.9	2.7	[4]
B	T.t.	15	1.8	5.1– 7.4	6.5	4.2	[g]
B	T.[f]	25	5	10.0–11.6	10.8	9.1	[g]
C	L.v.	20	10	5.4– 8.3	6.9	6.9	[14]
				5.2– 9.2[e]	7.2	5.9	

[a] $\dot{n}_{O_2}$ (20°C) is the weight specific rate of oxygen consumption at 20°C, calculated as

$$\dot{n}_{O_2}\,(20°C) = \dot{n}_{O_2} \times \theta_{exp} \times Q_{10} \times \frac{20-\theta_{exp}}{10};\ Q_{10} = 2.2$$

[b] $\dot{n}_{O_2}$ (10 mg) is the specific rate of oxygen consumption corrected for temperature (20°C) and individual weight ($_wW_{exp}$) and expressed for a standard individual of 10 mg $_wW$

$$\dot{n}_{O_2}\,(10\text{ mg}) = \dot{n}_{O_2} \times {}_wW_{exp} \times (10\text{ mg}/{}_wW_{exp})^{(b-1)};\ b = 0.75$$

[c] *Tubifex* and *Limnodrilus* in mixed samples

[d] Calculated rates for individuals of 10 mg and 1 mg according to the published weight-rate relationship

[e] 95% confidence limits of the mean

[f] *Tubifex templetoni*

[g] For references see [14]

possible at constant low oxygen concentration, ecologically meaningful information on physiological functions in a low oxygen environment remains elusive (see also Chap. II.2). Furthermore, the experimental oxygen regime is unidirectional in closed systems as opposed to fluctuating environmental conditions in nature, which can be simulated only in open flow respirometers.

Users of open-flow respirometers mention also the disturbing effect of accumulating excretory products on oxygen uptake, while users of closed systems ascribe little significance to this effect. These attitudes reflect the lack of experimental proof for either argument. Addition to the medium of 2 mmol dm^{-3} acetate, an endproduct excreted by several anoxic invertebrates, did not significantly influence the aerobic and anoxic rate of heat dissipation of *Lumbriculus* (unpublished observation). However, the role of accumulating excreta in supporting a high rate of bacterial respiration has also to be considered in closed respirometers.

As the pitfalls of closed systems become increasingly recognized, intermittent flow respirometers are coming into wider use ([1], Chaps. II.1, II.5), although a glance through the literature shows that for zooplankton the closed bottle method is still most commonly relied upon.

3 System Design Parameters of the Twin-Flow Respirometer

Just as the choice of a POS represents a compromise between stability, sensitivity, stirring requirements, and response time (Chap. I.1), so does any particular design of a respirometer involve certain compromises regarding (1) the sensitivity, (2) time resolution of oxygen uptake rates, (3) a more or less disturbing environment for the experimental animal, and (4) ease of construction and operation. The decisions are dictated by the specific application, by the desired accuracy, and by keeping costs low.

In describing the twin-flow microrespirometer, I will briefly specify the main arguments underlying the construction of the system. Their importance will become more readily apparent in the discussion of system functions and in some case studies. All constituent parts of the respirometer in contact with the experimental medium are made of stainless steel or glass with the exception of the microvalves, the coating of the stirring magnets, and the Teflon stoppers of the animal chamber. Plexiglas and other easily machinable materials with a high oxygen solubility and permeability must be avoided. High adaptability of every system component and exchangeability of the independent functional parts determined the design. While it proved almost impossible to reduce the cost of the apparatus without considerable detriment to functional parameters, the most expensive component – the time lost due to methodological weaknesses – can be eliminated for a wide range of applications beyond those mentioned in this article.

3.1 The Flow Regime

Many applications of POS in conjunction with flow respirometers in studies on small aquatic animals have been described ([3, 8, 9, 21, 23, 26, 30, 37, 39, 43], Chap. II.7). Calibration of the POS and measurement of oxygen uptake are usually achieved by an alternating water flow to the oxygen sensor, either directly from a water reservoir or after passage through the animal chamber. If calibrations are made only at the beginning and at the end of an experimental run, then the accuracy of the measurements is

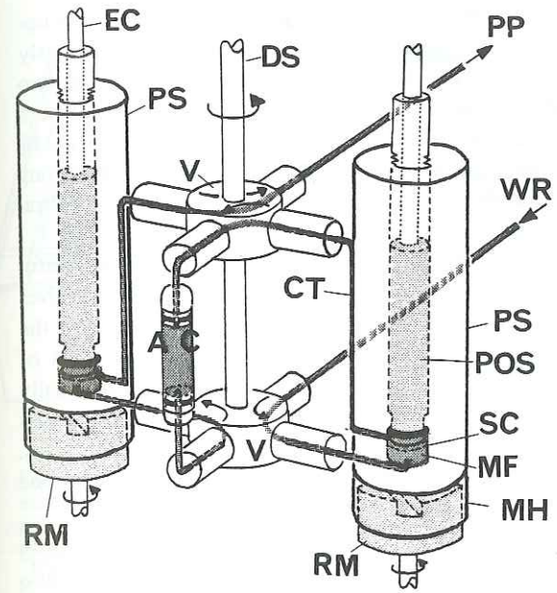

Fig. 1. The twin-flow microrespirometer. The flow regime is shown with the POS on the right hand side in the calibration position. The medium is pumped from the water reservoir (*WR*) to the first stirring chamber (*SC*) and POS by the lower four-way valve (*V*). The water flows upward through the stainless steel capillary tube (*CT*) along the side of the stainless steel POS sleeve (*PS*) and is directed by the upper four-way valve (*V*) to the animal chamber (*AC*) with flow direction downwards. Flow through the second stirring chamber with the POS in measuring position is symmetrical. The outlet of the upper valve is connected to the peristaltic pump (*PP*) by a Teflon tube. *DS* drive shaft, *EC* electrode cable, *MF* magnetic follower, *MH* stainless steel magnet housing, *RM* rotating magnet

limited by the nonlinear drift of the sensor signal. Intermittent calibration in these respirometers results in a discontinuous record of oxygen uptake and interrupts the flow of water through the animal chamber in most instruments. During calibration, the change in water current and the gradual oxygen decline may disturb the animals and interfere with internal rhythms.

These disadvantages do not apply to the twin-flow respirometer (Fig. 1). Due to the symmetrical arrangement of the two POS and measuring chambers, a continuous flow is maintained in a constant direction through the animal chamber (AC) and stirring chamber (SC) both during measurement and calibration. This is, in fact, the crucial requirement for simultaneous calorimetry, since the slightest change in pressure and flow through the animal chamber disturbs the calorimeter baseline. As the two four-way valves (V) are switched at the same time, the sensor previously in the calibration position (when water from the reservoir enters the stirring chamber directly) is set into the measuring position (water passes the other POS and the animal chamber before flowing into the stirring chamber), simultaneously the other POS is switched to the opposite position (Fig. 6). The POS switched to the measuring position shows, after some latency at an initial plateau, an overshoot which must not be mistaken for a fluctuation

in oxygen consumption (Fig. 8, POS 2). It is roughly proportional to the oxygen uptake rate (cf. Figs. 6 and 8) and is due to water from the stirring chamber (previously in the measuring position) and the capillary tubes connecting this chamber to the two valves, passing through the animal chamber for a second time (Fig. 1). Therefore a compromise has to be made between the advantage of frequent calibrations (every 2 h) with intermittent interruptions of the continuous record of oxygen uptake, and a long measuring and intercalibration interval (e.g., 12 h) with less certainty as to the calibration factor of the measuring POS.

Microvalves with minimum volumes (< 90 mm^3), as used in gas or liquid chromatography, are commercially available. In the present system two four-way valves (Pharmacia, LV4) are connected head to head. A central bore through the plug of the upper valve contains the drive shaft, which provides an easily accessible means of switching the two valves simultaneously (Fig. 1) either by hand or by an electronically timed motor. As the Pharmacia connections are vulnerable to damage by the stainless steel capillary tubes, there is always the danger of leakage and high diffusion rates. Hamilton valves (HVP 86779) provide a promising alternative, but no bore can be drilled through their plugs.

A LKB 10200 Perpex peristaltic pump with gear ratios of 1:200 or 3:250 is employed to keep the flow rate constant at chosen intervals between 3 and 25 cm^3 h^{-1}. The observed variability of maximally ± 0.7% may be largely due to errors in the measurement of the flow rate. With care taken to exclude evaporative loss of the water collected in a measuring cylinder, the long-term stability of flow rates within experiments was found to be 0.1%. Due to aging of the silicon rubber tubings, the flow rate changed much more between experiments. The connection of the pump to the outflow of the respirometer renders the precaution of oxygen diffusion into the peristaltic tubings unnecessary.

3.2 The Open-Flow Microrespirometer-Calorimeter

For simultaneous direct calorimetric and indirect respirometric measurement of metabolic activity, the twin-flow microrespirometer can be connected to an open-flow calorimeter (Fig. 2). At present, the best-suited commercial calorimeter for monitoring small animals is the LKB-2107 flow sorption microcalorimeter [13, 14]. The geometry of the heat detector system sets a restrictive upper size limit for the test animals. Optionally the LKB system can be equipped with a 0.5 cm^3 pyrex flow sorption chamber and a 1.4 cm^3 stainless steel flow ampoule. The latter, however, is not recommended for very accurate work due to problems associated with the standard calibration procedure [46]. The flow-through vessel is contained in an aluminum block, and in the case of the flow sorption chamber the gold outlet capillary tube is coiled to ensure perfect heat exchange in the calorimeter detector. Thus, any heat effect in the animal chamber builds up a temperature gradient across the thermopiles, which in turn gives rise to a voltage signal while the heat dissipates into the constant temperature heat sink of the calorimeter. The ratio of the measured potential and the heat dissipatet by the animals or by an electrical resistor (calibration heater) is the static gain value of the system, amounting to 0.055 μV μW^{-1} [13] or roughly 6 μV per 1 μmol O_2 h^{-1} consumed in aerobic metabolism.

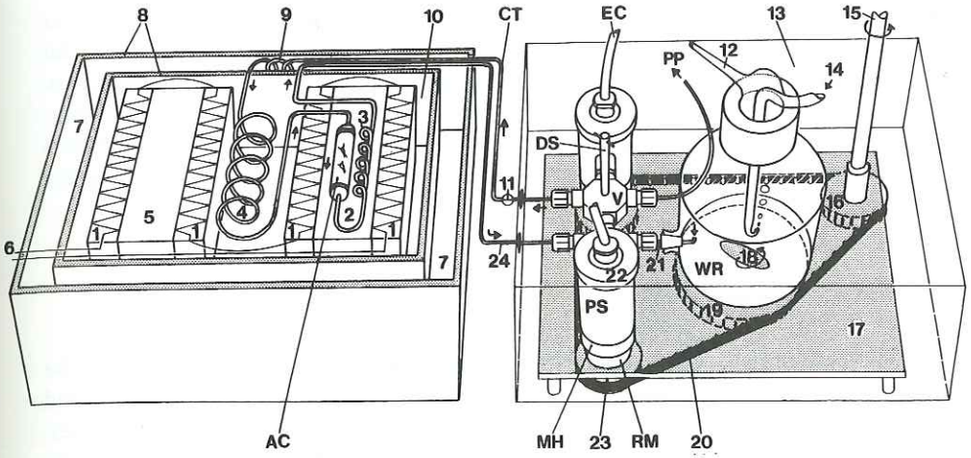

Fig. 2. The open-flow respirometer-calorimeter: the twin-flow microrespirometer (cf. Fig. 1) connected to the LKB-2107 flow sorption microcalorimeter. *AC* animal chamber, *CT* capillary tube, *DS* drive shaft for switching the two four-way valves, *EC* electrode cables of the POS, *MH* magnet housing of the bottom assembly of the stirring chamber, *PP* outlet Teflon tubing connected to the peristaltic pump, *RM* rotating magnet driving the magnetic follower in the POS-stirring chamber, *V* four-way microvalve, *WR* water reservoir for p_{O_2} equilibration. *1* thermopile, *2* heat detector, *3* detector heat exchanger (gold *CT*), *4* internal heat exchanger (gold *CT*), *5* static reference detector, *6* thermovoltage transducer cables connecting to the Keithley 150B microvolt ammeter, *7* constant temperature air bath of the calorimeter, *8* thermal insulation, *9* external heat exchanger (gold *CT*), *10* heat sink (aluminum block), *11* three-way microvalve connecting the stainless steel *CT* from the POS in calibration position with the gold *CT* to the animal chamber, *12* gas outlet, *13* constant temperature water bath of the respirometer, *14* gas line from the gas mixing pump to the water reservoir, *15* drive shaft connected to the synchronous motor, *16* gear wheel driving the toothed rubber belt, *17* lower mounting plate of the gear wheels and rotating magnets [the upper mounting plate (Fig. 3) is not shown here], *18* magnetic stirring bar in the water reservoir, *19* bracing wheel with impeller magnet, *20* rubber drive band, *21* stainless steel *CT* from the water reservoir to the POS, *22* retaining nut fixing the POS sleeve to the upper mounting plate (Fig. 3), *23* gear wheel (below mounting plate) driving the rotating magnet (above mounting plate), *24* capillary connection from the animal chamber to the POS in measuring position

The original Teflon inlet and outlet tubings of the calorimeter had to be replaced by gold capillary tubes to prevent gaseous diffusion and inhibit bacterial growth [13]. A three-way microvalve interpolated between the respirometer and the calorimeter inlet (Fig. 2) is advantageous during exchange of the animal chamber and for cleaning the apparatus. Inflow water is thermally equilibrated by passage through the external and internal heat exchangers before flowing through the animal chamber in the heat detector. The static reference detector compensates for all symmetrical disturbance effects of external temperature fluctuations. A symmetrical arrangement of the gold inlet and outlet capillaries is therefore necessary since the metal tubes enhance thermal leakage between the insulated heat sink and the calorimeter thermostat, and asymmetries result in diminished baseline stability. Since the drift of the calorimeter baseline as observed with high signal amplification (3 μV or about 5 μW recorder full scale) is correlated with the dynamic properties of the necessarily nonideal thermostat,

mathematical baseline correction procedures can be employed [27]. The flow of water through the heat detector shifts the baseline by some constant value as long as the flow rate and the viscosity of the medium are constant. Rapid switching of the respirometer four-way valves for POS calibration produces no disturbing effect whatsoever. Between experiments the oxygen sensors can be removed from the stirring chambers for electrolyte renewal and application of new membranes without disassembling any other part of the apparatus.

3.3 POS and Stirring Chamber

Various types of POS may be used with the twin-flow respirometer. A choice has to be made between small and large cathodes, in other words between stirred and unstirred POS (Chap. I.1). In preliminary experiments small-cathode sensors (Radiometer, E 5048/0) were sensitive to pressure and electrical interferences in a stopped-flow system. Hence a large-cathode POS (YSI 5331) was chosen and equipped with a minimum volume stirring chamber (Fig. 3). This sensor produces a current of 0.09 to 0.13 μA (air-saturated water at 12°C with the YSI standard membrane) which is easily converted into a voltage (R_L 100 kΩ, Chap. I.10) and displayed with a potentiometric compensation recorder. It proved practical to use the 300% zero suppression and set the calibration point at air saturation to about 90% of recorder full scale. The full scale deflection is then roughly equivalent to a change of 25% air saturation, and even high oxygen consumption rates should not reduce the oxygen content in excess of this limit, which would require resetting of the suppression range. After about 2 weeks of continuous operation, the signal of the YSI sensor usually becomes noisy and drifts off. This indicates that the electrolyte and membrane should be replaced. If the anode has turned dark it should be cleaned with a 25% ammonia solution.

Within the stirring chamber (Fig. 3) a strong and stable water current is generated at the POS membrane. At the same time the chamber acts as a centrifugal pump and exerts a pressure in the direction of throughflow (Fig. 4). The disk-shaped magnetic stirrer (Radiometer D 4030) displaces the major part of the volume of the stirring chamber and leaves just enough space to avoid resistance to the throughflow. At high rotation speeds, the minimum dead volume of the measuring chamber is also important to prevent wobbling of the stirrer.

Even at 30 rotations per second a stirring effect (0.06% per rotation/second) was observed. Therefore a synchronous motor (Papst, SZ 62.75-4-173 DeM/K-B357) is employed and the two rotating magnets (Fig. 1) are driven via a toothed rubber belt at a constant stirring speed of 25 rotations per second ($\triangleq$ 1500 rpm). A third rotating magnet is cast in an epoxy gear wheel which acts as the bracing wheel for the drive band and is of larger diameter than the other gear wheels. This magnet agitates the magnetic stirring bar in the water reservoir (Fig. 2) to enhance gas equilibration of the water (Chap. I.2) during changes in experimental p_{O_2}. The gear wheels and drive magnets are mounted on stainless steel shafts which rotate in waterproof ball bearings. The stirring assembly also provides vigorous mixing of the constant-temperature water bath which is essential for precise thermoregulation.

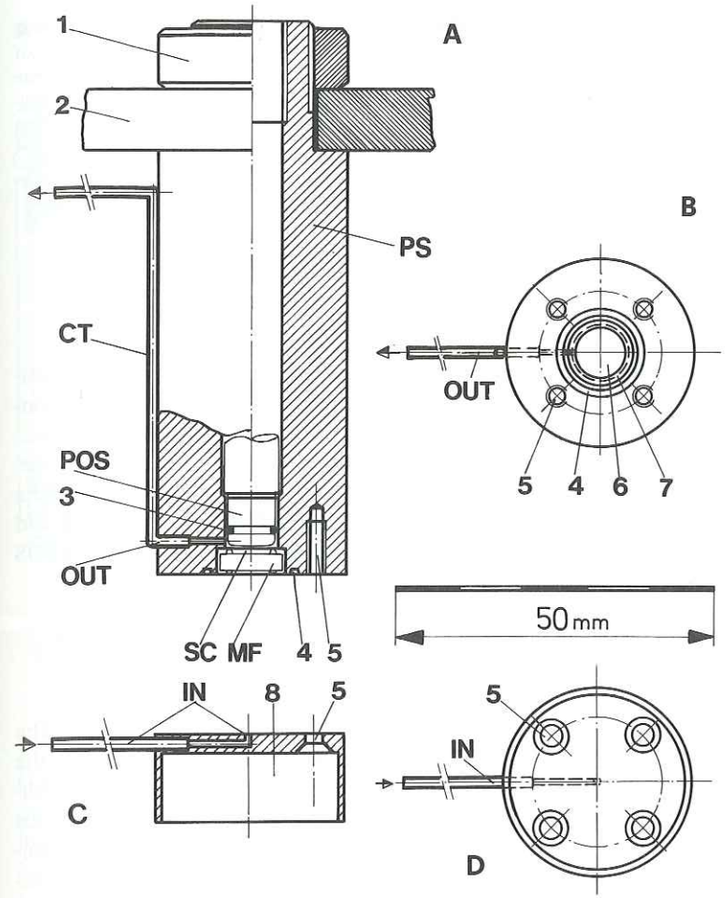

Fig. 3A–D. The stirring chamber. Cut view and cross-section of the POS sleeve (**A, B**) and the bottom assembly (**C, D**) respectively. *1* retaining nut, *2* Perspex mounting plate, *3* O-ring of the POS serving as a seal of the stirring chamber (*SC*), *4* O-ring groove for sealing the stirring chamber between POS sleeve and bottom assembly, *5* threaded hole for fixing the bottom assembly to the POS sleeve, *6* central bore of the POS sleeve, *7* stirrer guide, *8* drive magnet housing. Other symbols as in Figs. 1 and 2

An additional advantage of the stirring chambers warrants consideration. If the lower four-way valve (Fig. 1) is switched while the other valve is kept in a constant position, then the stirrer on the right-hand side maintains a flow through the animal chamber. In this way the open-flow system is changed into a closed-flow respirometer. The water flow is high at 25 rotations per second, despite the resistance of the capillary tubings and valves, and may be regulated by a needle valve interpolated between the four-way valve and the animal chamber. An open-flow current respirometer can be made by inserting a third stirring chamber (without POS) to produce a short-circuit flow (cf. Fig. 4).

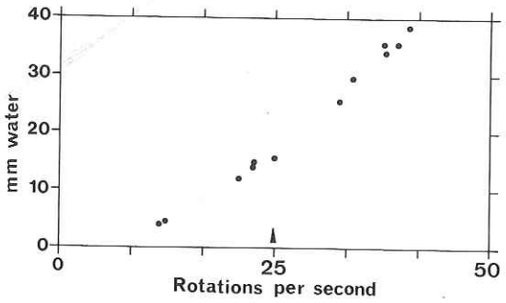

Fig. 4. Pressure exerted by the stirring chamber of the POS as a function of stirring speed as measured by the rise of the water column in a Teflon capillary tube (1 mm water = 9.80 Pa)

For some applications, however, rigorous stirring of the medium may not be feasible. The bottom assembly of the measuring chamber (Fig. 3C,D) may be used in conjunction with any other POS sleeve providing an O-ring seal. With a micro-cathode sensor (e.g. Chap. I.7) no magnetic stirrer is required. Then the unidirectional flow regime, irrespective of valve position, is especially advantageous, since the central bore in the bottom assembly leads the throughflow directly to the central cathode of the POS and minimizes oxygen depletion at the membrane. This is important even with some POS which are specified as "stirring-insensitive".

3.4 The Animal Chamber

The twin-flow respirometer can be connected to any type of animal chamber. The latter has to be adjusted in shape and in size to the experimental animal and to the desired range of flow rates. The animal chamber may also provide facilities for additional simultaneous measurements and may even be remote, such as in simultaneous direct and indirect calorimetric measurements (Fig. 2). The design of the animal chamber, however, is not as simple as it might at first appear to be. Every construction involves a compromise between minimum restriction of the animal and time resolution of oxygen uptake rates, since the volume and the pattern of water exchange in the animal chamber and the flow rate comprise the key factors determining the time response characteristic of a flow respirometer (Table 2).

Table 2. Interdependence of throughflow and volume of the animal chamber relative to animal size in determining the system specifications of a flow respirometer

		Volume		
		Large	Small	General
Flow	Low	Poor time resolution, large p_{O_2}-gradients	Reasonable time resolution	High accuracy
	High	Reasonable time resolution susceptible to animal behavior	Good time resolution, well-defined p_{O_2}	Low accuracy
	General	Unrestrictive	Restrictive	

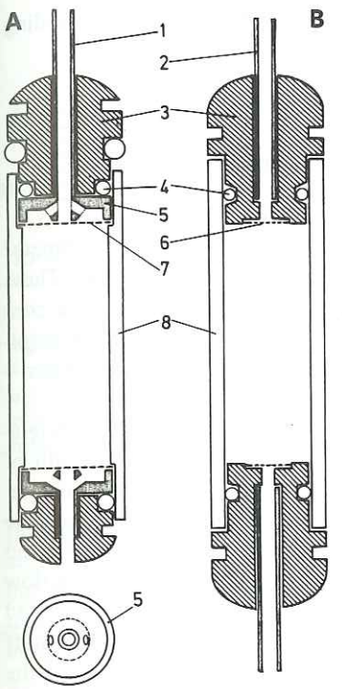

Fig. 5A,B. Animal chambers. **A** pyrex chamber of the LKB-2107 flow sorption microcalorimeter, 0.5 cm^3 volume. **B** similar glass chamber with the same inner dimensions for direct connection to the microrespirometer. *1* gold capillary tube, *2* stainless steel capillary tube, *3* Teflon cap, *4* O-ring, *5* gold nut, *6* Nickel grid (as used in electron microscopy), *7* nylon gauze, *8* glass tube

Generally two ideals may be approached for obtaining an optimum time resolution: (1) a capillary tube chamber without mixing, where a laminary flow of water extends over the whole cross-section; and (2) a chemostat vessel where the rate of mixing is high relative to the throughflow. In the latter case the chemostat theory applies and backcalculation of actual rates is possible using mathematical correction factors for the time course of oxygen concentration at the outflow (see below). The turbulence required for ideal mixing and the damping of the signal increase with increasing volume of the animal chamber, thus a small volume respirometer provides a more accurate time resolution. Both ideals can only be approached to some extent and are restrictive or disturbing to most animal species.

In the applications discussed below, the 0.5 cm^3 pyrex chamber of the LKB flow sorption microcalorimeter was used for simultaneous calorimetric and respirometric measurements (Fig. 5A). A similar glass tube chamber (Fig. 5B) served for independent applications of the twin-flow microrespirometer. However, for the simultaneous measurement of locomotory activity of microzooplankton a plain glass chamber of the same inner dimensions with side walls of stainless steel had to be constructed. This ensures an undistorted optical image of the animals (Gnaiger and Flöry, in prep.). These chambers allowed free locomotory movement of planktonic copepods.

In ecological bioenergetics, the aim is to determine oxygen uptake under natural, unrestrained conditions. The resolution of rapid changes in respiratory rate is then impossible and less important. In such studies large unstirred chambers provide the animals with as natural an environment as possible, and time averages of oxygen con-

sumption can be measured accurately despite the uncertainty which prevails regarding short-term fluctuations.

4 Precision and Accuracy in Static and Dynamic Analyses

The accuracy of oxygen uptake measurements with the twin-flow microrespirometer depends on several variables, last but not least on the skill of the experimenter. These variables will be discussed on the basis of experience gained under experimental conditions considered to be difficult, i.e., with factor combinations resulting in low respiratory rates (0.01 to 0.1 μmol O_2 h^{-1}), especially at low p_{O_2} (down to 4 mbar = 0.4 kPa or 2% air saturation).

Experiments were performed in a constant temperature room (17 ± 1°C) with relative air humidity of 30% to 65%. The respirometer was immersed in a water bath of 6 ± 0.02°C. The animal chamber was placed either in the water bath or for simultaneous heat dissipation measurements in the calorimeter at an identical temperature. The biomass in the experiments ranged from 0.7 to 5 mg dry weight. Millipore-filtered (0.45 μm) tap water was used as the experimental medium and was pumped at a flow rate of 5.7 cm^3 h^{-1} through the system. The water reservoir was continuously aerated or equilibrated with a gas mixture at a gas flow rate of about 8.5 dm^3 h^{-1} (Wösthoff gas mixing pump, 1SA 27/4). Since humid room air served as one component of the gas mixture, a special correction factor was employed for the calculation of p_{O_2} in solution (App. B).

4.1 Calibration Factor

The barometric pressure, ${}_bp$, was frequently recorded and interpolated. Hence the oxygen concentration of thermostated water entering the POS chamber in calibration position, c_{in}, is

$$c_{in} = S_s \times p_{O_2}, \quad (1)$$

where S_s is the solubility of oxygen at the experimental temperature [μmol dm^{-3} kPa^{-1}], and p_{O_2} is the experimental partial pressure of oxygen [kPa] (App. A and B). The calibration factor of the POS in terms of partial pressure, F_p [kPa μA^{-1}], is

$$F_p = \frac{p_{O_2}}{I_{in} - I_r}, \quad (2)$$

where I_{in} is the electrode signal corresponding to the calibration p_{O_2} at time t, and I_r is the residual (zero) current of the sensor [μA]. I_r amounted to 0.5 to 1.5% of the aerobic signal and can be estimated by the intercept of an I_{in}/p_{O_2} regression in experiments with several p_{O_2} levels. However, the variability of the "oxygen current", $I_{O_2} = I_{in} - I_r$, contributes to the variance of the intercept. In 10 experiments lasting for 1 to 3 days with 4 p_{O_2} levels (100%, 10%, 5%, 2% air) the 95% confidence interval of

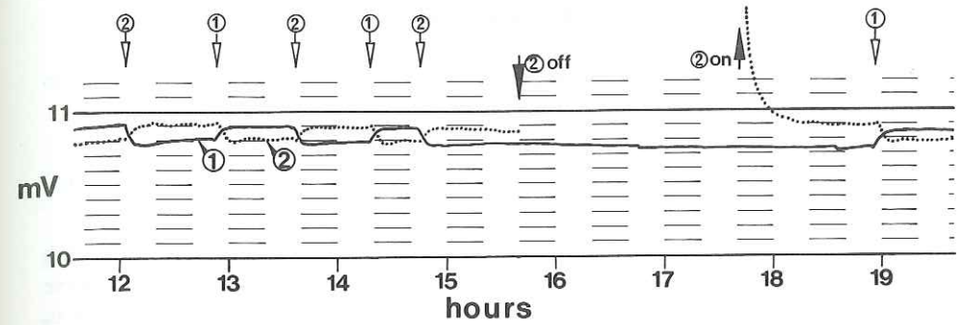

Fig. 6. Blank oxygen consumption run (12°C, air-saturated water, f = 5.9 cm^3 h^{-1}) recorded on a two-channel potentiometric recorder (10 mV ≙ 0.1 μA). Switching from measuring to calibration and vice versa is shown by *arrows* and the *corresponding numbers* indicate which POS is switched into calibration position. The polarizing voltage (0.8 V) of POS 2 in calibration position was intermittantly switched off (*black arrow off*), and on (*black arrow on*)

the intercept (= extrapolated I_r) ranged from 0.1% to 1.7% of the electrode current in air. This uncertainty affects calculations of aerobic respiratory rates by less than 1%, but becomes increasingly important at low p_{O_2}. Zero calibrations in Na-sulfite solutions made before mounting the POS in the respirometer are not recommended. In many cases these were considerably higher than calibrations made in the respirometer with pure nitrogen, where I_r was extremely stable once the steady state was reached. The instability of the calibration factor can therefore be attributed mainly to the variable oxygen current at constant I_r: frequent calibrations at experimental p_{O_2} are appropriate to cancel out this source of error (Fig. 6). Since the barometric pressure changes slowly with time, it is convenient to combine all changes in a concentration-based calibration factor, F_c [μmol dm^{-3} μA^{-1}],

$$F_c = \frac{c_{in}}{I_{in} - I_r}. \quad (3)$$

The signal of the POS in measuring position, I_{out}, is then simply converted to the oxygen concentration of the medium leaving the system, c_{out},

$$c_{out} = F_c \times (I_{out} - I_r). \quad (4)$$

The calibration factor will vary depending on the type of POS, the quality of the membrane and O-ring fit (Chap. I.1), ageing and poisoning of the cathode, anode and electrolyte (Chaps. I.2, I.5), and on bacterial growth on the membrane (Chap. II.9). In long-term tests from 40 to 120 h, the stability of the calibration factor was better than ± 2.5% under aerobic conditions. Occasionally following long anoxic periods, however, the signal of one POS did not stabilize for many hours or reached a steady state 15% higher than previously, while the other POS remained stable. This aberrant behavior remained unexplained (cf. Chap. I.4, control of membrane). Even for highly reliable POS, a sufficient stability < 0.2% can be achieved only with the aid of frequent calibrations of the undisturbed sensor, which is possible in the twin-flow system.

4.2 Oxygen Reduction Ratio, Blank Oxygen Consumption, and Oxygen Diffusion

The change in the amount of oxygen per unit time, $\dot{N}_{O_2}$ [μmol h^{-1}] is proportional to the flow rate, f [dm^3 h^{-1}], and the change in oxygen concentration,[2]

$$\frac{\Delta N_{O_2}}{\Delta t} = f \times (c_{in} - \bar{c}_{out}), \quad (5)$$

where $\bar{c}_{out}$ is the mean oxygen concentration in the POS chamber in measuring position during the time interval Δt. The time interval chosen has to be small relative to changes in barometric pressure, but large as compared to irregular fluctuations in c_{out} (see below). The oxygen reduction ratio, R_{O_2}, relates the concentration change to the input oxygen concentration,

$$R_{O_2} = \frac{c_{in} - \bar{c}_{out}}{c_{in}} = \frac{\bar{I}_{in} - \bar{I}_{out}}{\bar{I}_{in} - I_r}, \quad (6)$$

whence Eq. (5) becomes

$$\dot{N}_{O_2} = R_{O_2} \times c_{in} \times f. \quad (7)$$

S.D.(c_{O_2}), the relative standard deviation of the mean of consecutive steady-state measurements of c_{in} or c_{out}, was 0.12%. This results in a sensitivity of 3 nmol h^{-1} at a flow rate of 6.10^{-3} dm^3 h^{-1} (see Table 3). For comparison, the sensitivity of the Cartesian diver is 0.05 nmol h^{-1} [28] and the sensitivity of the flow microcalorimeter is 2 μW [13], equivalent to about 16 nmol O_2 h^{-1}.

Table 3. Relative standard deviation of oxygen uptake measurements [%] as a function of R_{O_2} and S.D.(c_{O_2}). From [37]

R_{O_2}	S.D.(c_{O_2}) [%]			
	0.1	0.5	1	2
0.05	2.8	14.0	28.0	55
0.10	1.3	6.7	13.0	27
0.15	0.9	4.4	8.7	17
0.20	0.6	3.2	6.4	13
0.25	0.5	2.5	5.0	10

The calculation of respiratory rates of the experimental animals, however, is complicated by the side effects of blank oxygen consumption and oxygen diffusion, so that confidence limits of animal respiration cannot be ascertained with the same accuracy. The oxygen consumption by the relatively large cathode of the POS is about 1 nmol h^{-1} under aerobic conditions, which is below the detection limit (Fig. 6). The aerobic blank oxygen consumption rate also could not be fully explained by bacterial

2 Although a negative value should be assigned to the amount of oxygen removed within a system, the convention of reporting oxygen uptake rates as positive values is adopted here for convenience. Hence oxygen diffusion into the system (which should be positive) is negative in this context

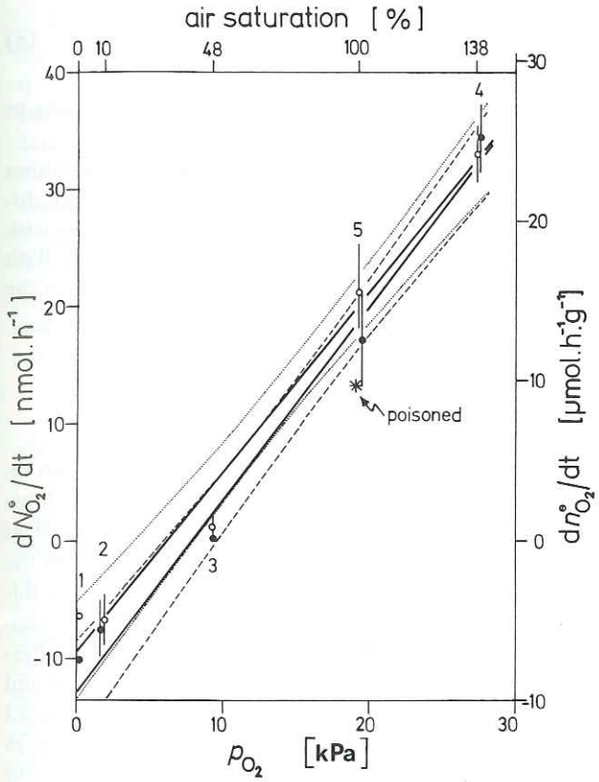

Fig. 7. Blank oxygen consumption as a function of p_{O_2} in experiment RJC1 after removing the animals from the animal chamber. The changes in oxygen are expressed as absolute rates, $dN^{\ominus}_{O_2}/dt$, and as $dn^{\ominus}_{O_2}/dt$ which is the blank rate relative to the dry weight of the animals whose oxygen uptake was recorded for 95 h (see Fig. 12). The blank rates were observed from 97 to 377 h in the following sequence of air saturation values: 100-48-138-100-48-10-0-100. The negative sign indicates net oxygen diffusion into the system. *Open* and *closed circles* are the means, and the *dotted* and *broken lines* are the 95% confidence limits of the two regression lines for POS 1 and POS 2 respectively [$\dot{N}^{\ominus}_{O_2}$ (POS 1) = $-9.52 + 1.530 \times p_{O_2}$; $\dot{N}^{\ominus}_{O_2}$ (POS 2) = $-13.21 + 1.649 \times p_{O_2}$]. The *bars* represent the standard deviations of the means. The number of readings before and after calibration is indicated. The *arrow* points to the blank oxygen consumption obtained 20 h after poisoning with formaldehyde (4%)

respiration, as antibiotics or poisons exerted only a slight effect on the blank rate (Fig. 7). In 18 experiments with planktonic copepods the blank averaged 22 ± 5 nmol h^{-1}, but reached extraordinarily high values above 50 nmol h^{-1} in other cases. Hence the blank has to be determined and subtracted from the total rate for every experiment to achieve a precision better than 5% for an animal respiratory rate of 100 nmol h^{-1}. In studies of the rate/p_{O_2} relationship the blank rates have also to be determined at several p_{O_2} levels. Below 30%–50% air saturation oxygen diffusion into the system exceeded the chemical and biochemical processes of oxygen removal in blank runs. A least-squares regression gives a good estimate of the blank rate, which is a linear function of p_{O_2} (Fig. 7). By subtraction we obtain the specific rate of oxygen consumption, $\dot{n}_{O_2}$ [μmol h^{-1} g^{-1}], by the experimental animal(s) with total weight, W,

$$\frac{\Delta n_{O_2}}{\Delta t} = (c^{\ominus}_{out} - \bar{c}_{out}) \frac{f}{W}, \quad (8)$$

where $c^{\ominus}_{out}$ is the oxygen concentration of the outflowing medium corresponding to the blank rate determined at or calculated for the experimental p_{O_2}.

When the water bath was thoroughly flushed with nitrogen, the apparent diffusion rate at $p_{O_2} = 0$ could be reduced to zero. Without an isoperibolic oxygen jacket, diffusion rates averaged -12 ∓ 6 nmol h^{-1} in the last 8 experiments in conjunction with the calorimeter, corresponding to $c^{\ominus}_{out} = 2$ μmol dm^{-3} or 0.6% air saturation. With less experience, however, diffusion rates of -10 to -30 nmol h^{-1} were typical for the respirometric system alone using Pharmacia valves.

4.3 Two POS for Twin Measurements

So far the evaluation of the precision of respiratory rate measurements has been restricted to the analysis of the signal of a single sensor. With the twin-flow system, however, two independent measures of the oxygen concentration ratio are obtained at intervals (Fig. 8). Agreement between these twin measurements tends to confirm the above analysis. The absolute difference between the blank oxygen consumption or diffusion rates as measured by the two sensors was 2.5 ± 2.2 (S.D.) nmol h^{-1} in 25 control runs at p_{O_2} from 0 to 280 mbar (0–28 kPa, 0%–140% air saturation). The difference may in part be due to slight asymmetries in the sites of oxygen consumption and diffusion. Therefore, the rates of the blank obtained for each sensor were subtracted from the respective total consumption rate, although the regressions for the two POS were not significantly different (Fig. 7). This comparison indicates that an estimated sensitivity of 3 nmol h^{-1} for a single sensor system may be on the optimistic side, while the sensitivity is improved by taking the mean of the two respiratory rates [Eq. (8)] obtained with the twin-flow system.

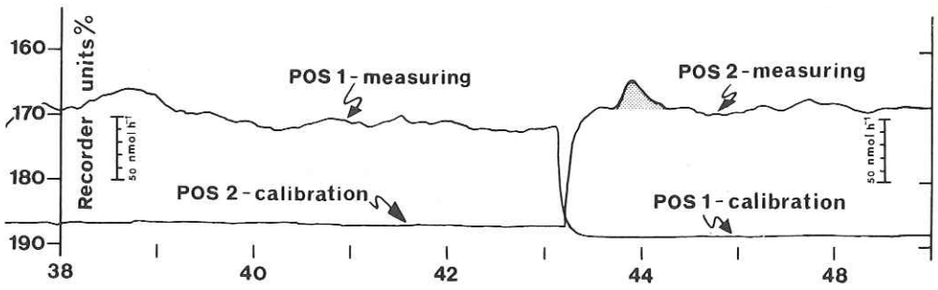

Fig. 8. Recorder traces of the two POS before and after switching the four-way valves of the twin-flow microrespirometer, in an experiment with 40 *Cyclops abyssorum* in the calorimeter chamber (experiment RJC1, 100% air saturation, see also Fig. 12). The hatched area is due to a second passage of some water through the animal chamber and stirring chamber after switching the POS into measuring position

Another at least equally important advantage of the twin-flow microrespirometer is the provision of objective criteria for the discrimination between normal and irregular system function; one may reject "bad data" on two levels: (1) If the calibration factor varies in a manner which renders the correction by interpolation impossible, then the data are bad for a functionally obvious reason. (2) If the twin measurements of respiratory rate disagree, then something must have been wrong for not necessarily obvious reasons. A third rejection criterion is provided by simultaneous calorimetry: scepticism is warranted if the ratio of oxygen consumption/heat dissipation shifts irregularly (see below). Objective discrimination between reliable and unreliable data is a potent means of reducing variability due to intermittent instrumental malfunction. This considerably enhances the significance of long-term experiments, especially as these cannot be repeated very often for reasons of time.

4.4 Response Time and Correction for Instrumental Lag

The dynamics of respiratory rates are a sensitive indicator of an animal's physiological state. Hence the accurate resolution of short-term patterns of oxygen uptake may be just as significant in analytical tests as the comparison of average oxygen uptake levels [18]. However, due to the inertia of a respirometer, true instantaneous rates may differ considerably from the apparent rates which are directly obtained from the untreated oxygen records (Fig. 8). This has usually been neglected [12]. The magnitude of the time delay and damping of *internal* changes in respiratory rate is not directly obvious, while after *external* changes of p_{O_2} the equilibration time of a respirometer is evidenced by the nearly exponential time course of the oxygen records (Fig. 9). The transient response of a respirometer reflects the dynamic properties of the various constituent parts which determine the over-all time behavior of the system (Fig. 9). On the basis of this information, suitable means can be contrived to alleviate the problem of inertia, where possible, by improving the physical characteristics of the most sluggish system component, or otherwise by correcting the observed values with tested mathematical models.

The response time, $\tau_{99\%}$, of the YSI sensor varied from 60 to 90 s, and steady state was reached within 200 to 400 s after transfer from air into Na_2SO_3 solution at room temperature. Old sensors should be discarded, if, despite a tight membrane fit and cleaning and regenerating the anode, equilibration times become very long (Fig. 9, curve 1). In the stirring chamber (Fig. 3) the response time of the POS is not limited by the thickness and the diffusion coefficient of the membrane and electrolyte layer (Chap. I.1), but depends primarily upon the flow rate, and on the mixing and the volume of water in the measuring chamber and the inlet flow tube. The 99% response time after switching the four-way valves ranged from 15 to 30 min, apparently increasing with a larger step change in p_{O_2} (Fig. 8, POS 2; Fig. 9, curve 2). A transit time elapses from the initial p_{O_2} change in a defined section of the respirometer (water reservoir, valve, first stirring chamber or animal chamber) until the POS starts to react. For simplicity this purely additive delay in the system's transfer function was always eliminated in the various expressions of time behavior.

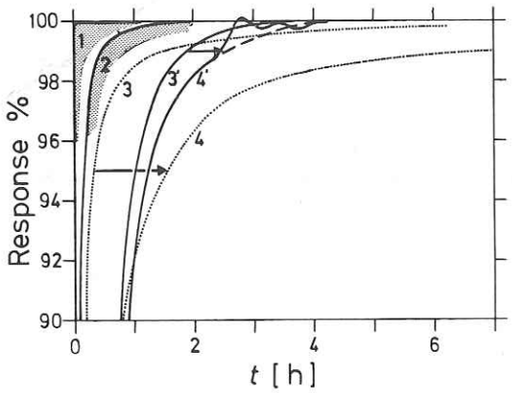

Fig. 9. The transient response to external p_{O_2} changes of functional components of the respirometer at different levels of integration at a flow rate of 5.7 cm³ h⁻¹. *1* POS after transition from air to Na-sulfite solution; the response of defective sensors is delayed (*shadowed area*), *2* POS in the stirring chamber after switching from measuring position (86% air saturation) to calibration position (100% air saturation). A delay of the response (*shadowed area*) indicates the trapping of gas bubbles in the flow system. *3* and *3'* POS in calibration position after changing the p_{O_2} of the gas equilibrating the 0.4 dm³ water reservoir. *3* change from air to pure nitrogen at a high gas flow rate. *3'* change from 10% O_2 in N_2 (= 48% air) to 10% air in N_2 at a lower gas flow rate. *4* and *4'* POS in measuring position corresponding to curve 3 and 3' respectively; both curves are corrected for the transit time due to the flow path from the first to the second stirring chamber (0.60 h with the animal chamber in the calorimeter). *4* the pyrex chamber in the calorimeter contained 40 dead specimens of *C. abyssorum* after poisoning (experiment RJC2, see Fig. 15); the O_2 concentration change was −326 μmol dm⁻³ during the first hour. *4'* the animal chamber in the calorimeter contained 40 active specimens of *Cyclops* (experiment RJC1, see Fig. 12); the O_2 concentration change was −120 μmol O_2 dm⁻³ during the first hour; irregularities are due to fluctuations in oxygen consumption by the animals

The instantaneous events taking place at the inflow of the stirring chamber can be calculated from the recorded values and from the exponential transient response curves (Fig. 9) by employing mathematical deconvolution methods [2, 38]. However, the response time of the POS in the measuring position depends predominantly upon the turbulence and the volume of water in the animal chamber which exceeds the volumes of the stirring chambers by a factor of about 20. In an unstirred animal chamber not only the geometry, but also the activity, position, and size of the animal(s) determine the effective dead volume and the distribution of throughflow. This precludes the use of invariant time constants for the resolution of the immediate respiratory response to an externally varied oxygen regime, since the physical effects of animal behavior are highly variable. This is illustrated by the different time lags between curves 3 and 4, and 3' and 4' in Fig. 9 (arrows) where equilibration is considerably enhanced by the locomotory activity of the live animals. Attainment of the final equilibrium and the form of the response curve also depend on the magnitude of the external p_{O_2} variation: only after large concentration changes does the amount of back diffusion from or into the oxygen-permeable materials exceed the limit of detection.

With this in mind, a pessimistic picture emerges regarding the applicability of simple mathematical models to improve the time resolution. However, these *internal* oxygen

changes are an order of magnitude below the *external* transient changes analyzed in Fig. 9. They never exceeded 25 μmol dm⁻³ during 1 h and were usually below 6 μmol dm⁻³ in a 0.3-h period (Fig. 17), whence higher-order exponential terms (necessary to describe curves 4 and 4' in Fig. 9) become less significant. Fry [12] considered a first-order model as applied to the mixed reactor (chemostat) to correct for the lag in open-flow fish respirometers [10]. Equation (5), including the lag term, then becomes

$$\frac{dN_{O_2}}{dt} = \frac{dV}{dt} \times (c^{\ominus}_{out} - c_{out}) + V \times \frac{dc_{out}}{dt} \quad , \tag{9}$$

where $dV/dt = f$ [dm³ h⁻¹], V [dm³] is the homogeneously mixed volume of the respirometer, and dc_{out}/dt [μmol h⁻¹] is the instantaneous rate of change in oxygen concentration of outflow water. The ratio of the system's storage and flow parameter is the time constant, τ [h],

$$\tau = \frac{V}{f} = \frac{V}{dV} \times dt, \tag{10}$$

or the period whereafter the response has completed 63% [35].

None of the simplifying assumptions inherent in Eq. (9) holds for a flow microrespirometer. Especially in conjunction with the flow calorimeter, the capillary connections from animal to measuring chamber contain a significant volume of water (2–3 cm³) in which oxygen fluctuations are damped due to the parabolic current profile and diffusive oxygen exchange between different water layers in laminar flow. Additional terms are required for the description of such a cascade system [2, 34]. But with an unstirred animal chamber the primary problem hinges on the changing and nonlinear effect of animal behavior on the transfer function of the whole system. Poor mixing in the animal chamber reduces the effective volume and the first-order time constant [Eq. (10)], and hence the outflow water transmits oxygen changes in the flow path more quickly. But at the same time a quite unpredictable high-order system is generated due to the slow and irregular interchange with the residual dead volume. This makes the significance of any refined deterministic model questionable. A first-order approximation was therefore considered, where all response characteristics (high-order, nonlinear) are lumped in a single, empirical time constant [35]. While according to Eq. (10) and using the volume of the animal chamber the theoretical time constant is calculated as 0.09 h, the transient response as obtained with active animals in the respirometer-calorimeter suggests a time constant ranging from about 0.2 to 0.3 h (Fig. 10). This is the period corresponding to the break frequency above which the amplitude ratio (the static gain value) and the phase response of the output signal fall off relative to the real fluctuations in oxygen uptake. With inactive animals this period is quite different, and high frequency fluctuations of the output signal may be artifacts due to movements only. Thereforth apparent oxygen consumption rates were averaged over 0.33 h intervals and no better time resolution was attempted.

The simultaneous measurement of heat dissipation and oxygen consumption provides the unique possibility of "calibrating" the transfer function of the twin-flow microrespirometer relative to the response time of the flow calorimeter in different experimental situations. The calorimeter time constant was determined at 120 to 150 s

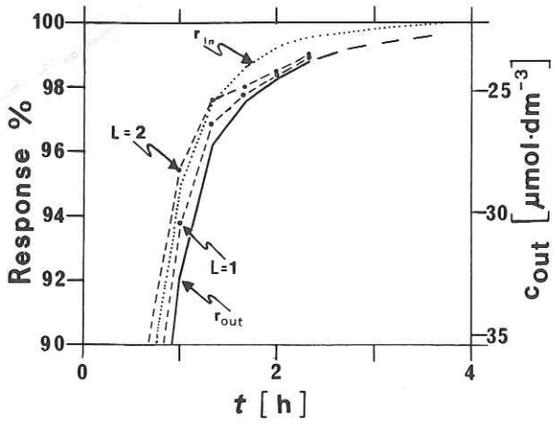

Fig. 10. Correction of time lag in the transient response to external p_{O_2} changes. The observed input transient (*dotted line*, r_{in}) and the observed output of the POS in measuring position (*full line*, r_{out}) correspond to curves 3' and 4' respectively of Fig. 9. The *dotted lines* are the corrected r_{out}-curves, r_{cor}, according to the equation [cf. Eq. (11)]

$$r_{cor} = r_{out,t} - \frac{L}{\Delta V} \times (r_{out,t-1} - r_{out,t}) \cdot$$

Two boundary values for the lag factor, L [cm³], were inserted as shown in the figure. The lumped first-order time constant is $L/(\Delta V/\Delta t)$; above the 97% response the significance of high-order terms becomes evident. The time constant is calculated by inserting r_{in} instead of r_{cor} in the above equation and solving for L

by electrical calibration and was not corrected for. The validity of considering a first-order correction for the respirometer can already be gauged from the generally high correlation coefficients of the untreated calorimetric and respirometric data. With more than one significant time constant relative to the calorimeter response, much larger deformations of the oxygen uptake record would be expected. However, the correlation coefficient could be optimized (Fig. 11) by adjusting the storage term or lag factor in the following difference equation [cf. Eq. (9)],

$$\frac{\Delta N_{O_2}}{\Delta t} = \frac{\Delta V}{\Delta t} \times (c^{e}_{out} - \bar{c}_{out,t}) + L \times \frac{(\bar{c}_{out,t-1} - \bar{c}_{out,t})}{\Delta t} , \qquad (11)$$

where Δt [h] is the time interval, $\bar{c}_{out,t-1}$ and $\bar{c}_{out,t}$ [µmol dm^{-3}] are the average oxygen concentrations of outflow water in successive time intervals, t−1 and t, respectively, and L [dm³] is the empirical lag factor (Fig. 10). The lag factor as adjusted relative to the calorimeter response will be indexed as L_c. The calibration of L_c (Fig. 11) rests on the assumption that the averages of the calorimeter output per 20 min accurately reflect fluctuations in aerobic metabolism, and that peaks of heat dissipation are not due to intermittently activated anoxic processes. The effects of likely deviations from this assumption on estimating L_c have to be critically examined for each situation (see below). The magnitude of the lag factor (the effective storage volume of the respirometer) estimated in the transient response analysis (Fig. 10) and the optimization of L_c with

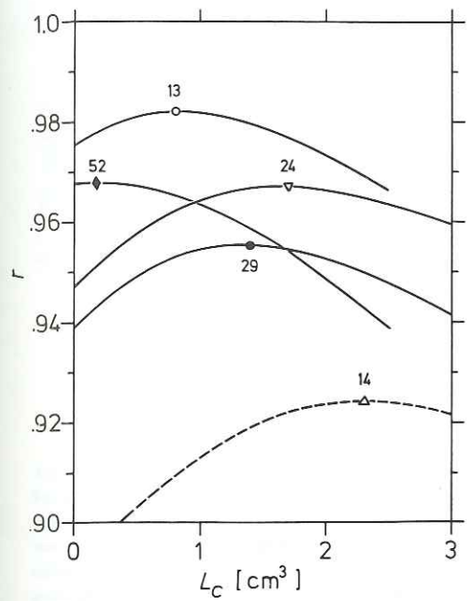

Fig. 11. Variation of the lag factor, L_c [Eq. (11)], for the construction of optimum curves of the correlation coefficient, r, between simultaneous calorimetric and respirometric measurements averaged over 0.33 h periods. *Open symbols* with one specimen of *Salvelinus alpinus* in the post-hatching stage under aerobic (*circle*) and hypoxic conditions (see Fig. 18 to 20). *Closed symbols* with 40 specimens of *Cyclops abyssorum* in the adult and copepodite V stage under aerobic (*circle*) and hypoxic conditions (see Figs. 15 to 17). The number of subsequent 20-min intervals for each experimental situation is given in the figure

different animal species and numbers (Fig. 11) agree well. This suggests the suitability of the approach. Actual rates of the test animals used may be expected to fall in the range of corrected rates corresponding to lag factors between 0.5 and 1.5 cm³ [Eq. (11)]. However, no statistical confidence intervals can be estimated. Standardized mixing of the animal chamber, digital data acquisition, and more realistic models are necessary to improve the above analysis.

5 Applications of the Twin-Flow Microrespirometer

In order to avoid giving the impression of an exaggerated emphasis on methodological details (which have too often been disregarded), we shall briefly inquire into some of the applications of the twin-flow microrespirometer. Case studies are presented to illustrate the practical advantages of the design and to demonstrate the importance of careful data analysis.

5.1 Oxygen Dependence in Open-Flow Respirometry

The physiological response of a population of *Cyclops abyssorum* from Kalbelesee (see Chap. III.1) to a hypoxic environment was investigated in long-term experiments. Oxygen uptake as a function of p_{O_2} and time after collection is shown in Fig. 12. The respiratory rate decreased exponentially independent of oxygen concentration. Only

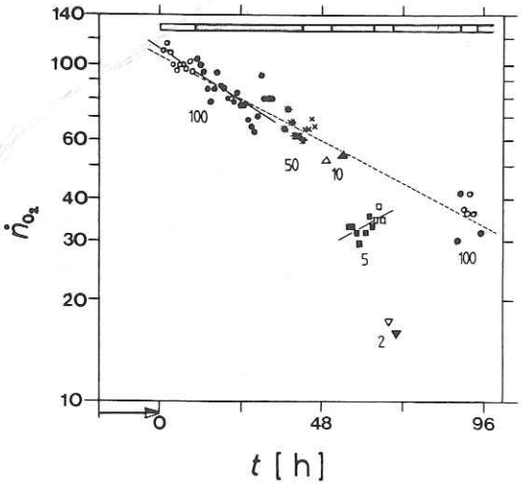

Fig. 12. Oxygen uptake, $\dot{n}_{O_2}$ (μmol h^{-1} g^{-1} dry weight), of *Cyclops abyssorum* as a function of time, t [h], and externally varied p_{O_2} (numbers in % air saturation) experiment RJC1: 1.36 mg total dry weight, 6°C; constant flow of 5.75 cm^3 h^{-1} through the respirometer-calorimeter; see also Figs. 7 and 8). The *arrow* on the time axis indicates the period between sampling the animals from lake Kalbelesee and the beginning of the experiment. The *broken line* is the least-squares interpolation of initial and post-hypoxic rates at air saturation. The *full lines* indicate the calculated exponential slopes of aerobic decrease and hypoxic increase, respectively, of oxygen consumption. The flow regime determining the successive periods in measuring and calibration position of a POS is shown by the *light* and *dark bar* on the top and by different symbols for the hourly averaged rates

after the transition from 10% to 5% air saturation of the inflow water did oxygen uptake immediately drop to half of the preceding rate. During the subsequent recovery period, oxygen consumption gradually approached the same level as that extrapolated from the initial aerobic rates, and nearly abolished the oxygen-induced change. Short-term acclimation to severe hypoxia is also seen in Fig. 15. These trends, uniquely resolved in an open-flow system, draw attention to the misleading picture which would inevitably result from this experiment if a closed respirometer were used (Fig. 13). In a closed system of large volume, the instantaneous starvation effect on the diminishment of oxygen uptake is obscured by the apparent dependence on the simultaneously reduced oxygen content. With a small volume and consequently rapid oxygen depletion, however, the acclimatory response to the varied oxygen regime remains elusive.

5.2 Hypoxia, Respiration and Activity

Oxygen uptake and locomotory activity were measured as a function of p_{O_2} and laboratory stress with 40 *C. abyssorum* in a 0.5 cm^3 plain glass animal chamber (Gnaiger and Flöry, in preparation). Active animals moved freely in the water column, but showed an oxygen-dependent tendency to attach to the walls of the animal chamber, while inactive specimens lay motionless on the bottom. The distribution of animals be-

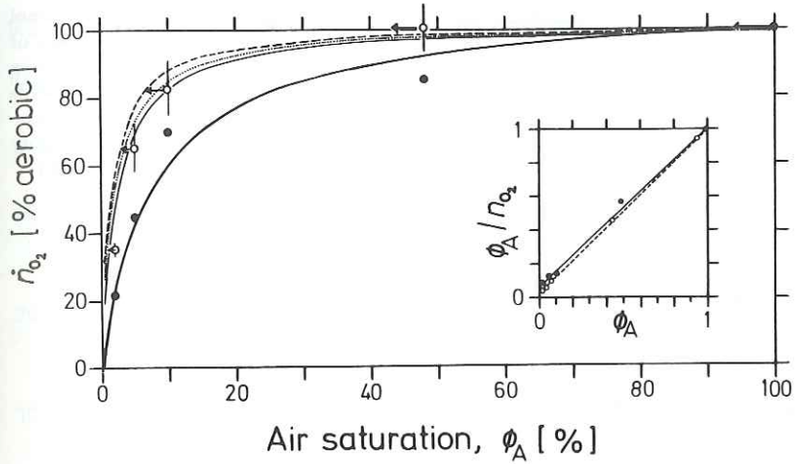

Fig. 13. Oxygen uptake, $\dot{n}_{O_2}$ (in % of the aerobic rate), as a function of air saturation, ϕ_A, and linearization of the $\dot{n}_{O_2}/\phi_A$ plot (*inset*) (experiment RJC1, see Fig. 12). *Full line* the average of aerobic rates (12 h before the external p_{O_2} change) is taken as the static aerobic reference value, and the inflow water represents the experimental conditions. *Other lines* the rate/time regression of aerobic oxygen consumption (Fig. 12, dotted line) served as a time correction for the aerobic reference value, and the p_{O_2} of inflow water (*right line with arrows*), outlfow water (*left line*), or the mean of the two (*middle line*) was used in the calculations

tween water column (N_c), walls (N_w), and bottom (N_b) was observed during prolonged periods of constant controlled oxygen conditions. From this distribution an index of relative activity,

$$\frac{N_c + f_w \times N_w}{N_c + N_w + N_b} \qquad (12)$$

could be contrived, where $N_c + N_w + N_b$ is the sum of individuals in the respirometer, and f_w is a weighting factor for the number of animals intermittently attached to the walls, which expresses their state of activity relative to the unrestricted activity of free-swimming animals. f_w can also be considered as an expression for the artificial effect of confinement of planktonic animals in a small volume chamber. It was derived by linearizing the oxygen consumption/activity relationship at various p_{O_2} levels between 100% and 2% air saturation (Fig. 14). The intersect of this plot with the ordinate agrees well with the relative activity observed under anoxic conditions, while the negative intersect with the aerobic respiration axis hints at the level of anoxic metabolism in sustaining physiological functions in the low p_{O_2} range.

5.3 Simultaneous Respirometry and Calorimetry

The twin-flow microrespirometer was primarily designed for the establishment of a simultaneous direct and indirect calorimetric method (Fig. 2), and herein appears its most promising and innovative field of application. Within the pratical context of this

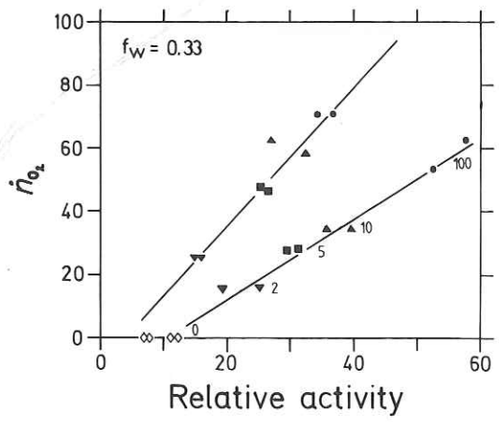

Fig. 14. Oxygen uptake, $\dot{n}_{O_2}$ (μmol h^{-1} g^{-1} dry weight), as a function of locomotory activity and air saturation (numbers in %) in two experiments with *Cyclops abyssorum* (40 individuals) at different levels of "laboratory stress" (Gnaiger and Flöry, in prep.)

book, however, I want to point out some of the problems encountered in operating simultaneously, over several days, and near the limit of detection, two instruments, both of which are dependent upon the continuous function of a number of mechanical and electronic components (Fig. 15). However, unique advantages are provided by the simultaneous measurement of both oxygen uptake and heat dissipation: an erroneous result with one apparatus is very likely to become apparent by comparison with the other. The second case study with salmonid fish larvae (Fig. 18) demonstrates the fascinating results that remunerate the considerable effort and expense invested. Some speculative comments suggest the broad spectrum of questions which can be solved or, even more important, may be unexpectedly introduced, by the application of the open-flow microrespirometer-calorimeter.

In one series of experiments the calorimeter baseline did not stabilize due to evaporative heat loss in the heat detector. Only after the time course of oxygen uptake and heat dissipation coincided was there evidence of the final diminution of this interfering effect (Fig. 15). In the same experiment 12 out of 40 *C. abyssorum* were egg-carrying females. Nauplii were washed out as they hatched, and some were observed in the collecting cylinder. Nauplii are intolerant to anoxia (from hour 68 to 87, Fig. 15). Upon return to aerobic conditions, the apparent oxygen uptake increased steadily, while heat dissipation even decreased after an initial overshoot. This implausible discrepancy motivated the application of antibiotics in detecting possible bacterial decomposition of dead nauplii trapped in the capillary system. As expected, the respirometric signal inflected immediately, to converge with the calorimeter output after 27 h. This suggests that the bacterial interference was by this time largely under control. The disturbed pattern of heat dissipation indicates a significant effect of the antibiotics on the animals. Much valuable information is revealed even in such a "faulty" simultaneous experiment: although the drift of the calorimeter baseline was uncontrolled but steady (during the first 48 h in Fig. 15), the fluctuations in heat dissipation could be compared quantitatively with the instantaneous respiratory rates during different sections of the experiment. There was a remarkably close correlation between the regular fluctuations in heat dissipation and oxygen uptake (Fig. 16). This

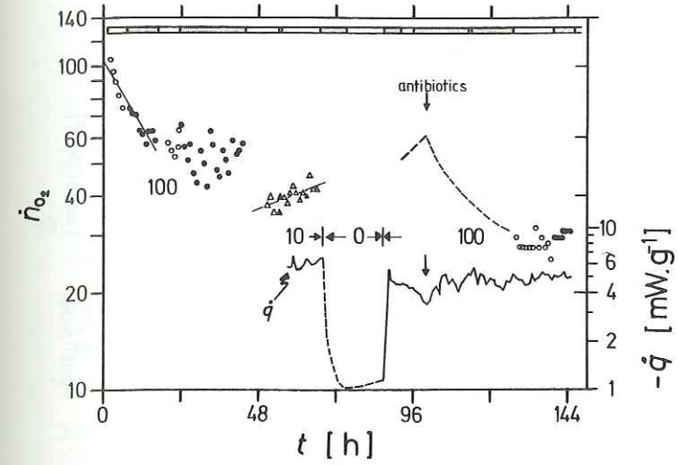

Fig. 15. Oxygen uptake, $\dot{n}_{O_2}$ (μmol h^{-1} g^{-1} dry weight), and heat dissipation, $\dot{q}$ (mW g^{-1} dry weight), of *Cyclops abyssorum* as a function of time, t [h], and externally varied p_{O_2} (experiment RJC2: 1.418 mg total dry weight; 6°C; at constant flow of 5.65 cm^3 h^{-1}). See Fig. 12 and text for further explanations

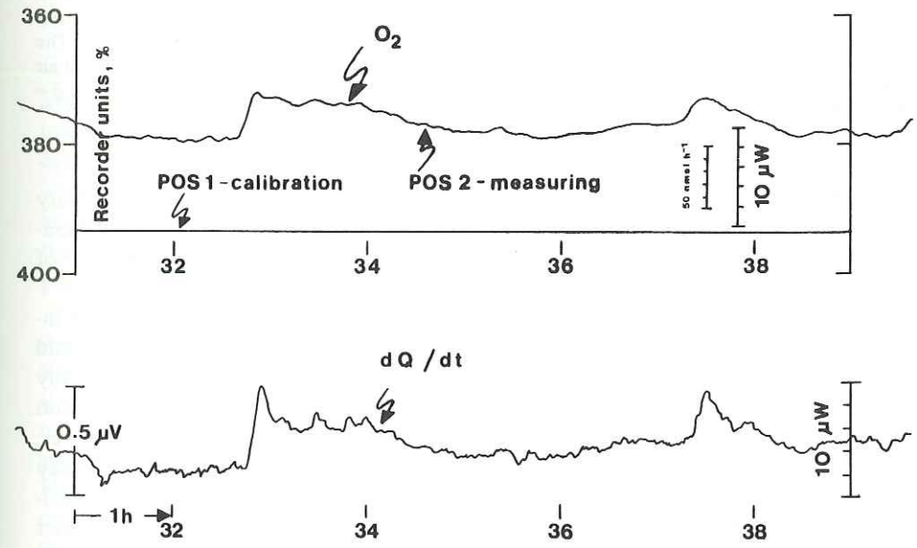

Fig. 16. Recorder traces in a simultaneous calorimetric and respirometric experiment showing the activity pattern of a group of 40 specimens of *Cyclops abyssorum* (experiment RJC2, see Fig. 15). The p_{O_2} record of the POS in measuring position is shifted backwards relative to the calorimeter power-time curve by 11 min to correct for the transit time in water flow from animal to stirring chamber

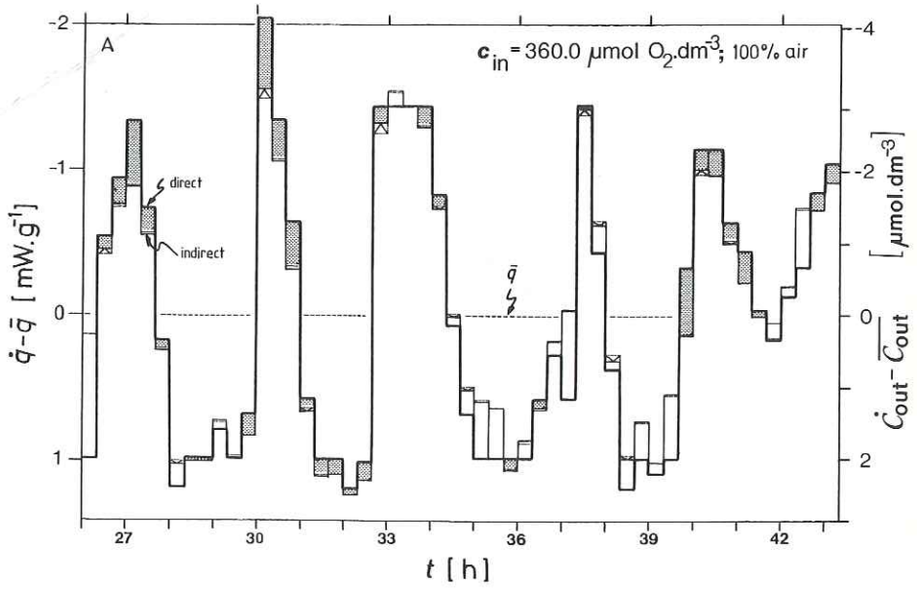

Fig. 17. Pattern of heat dissipation and oxygen consumption expressed as the deviations from the mean value, $\bar{q}$, during the period shown (experiment RJC2, see Figs. 15 and 16). *Full line* 20-min averages of the direct calorimetric rate corrected for baseline drift. *Thin line* 20-min averages of oxygen uptake expressed as heat dissipation on the basis of the theoretical oxycaloric equivalent of −450 kJ (mol O_2)$^{-1}$ (App. C); the corresponding changes in oxygen concentration of outflow water are indicated on the right hand side. Changes within 20 min did not exceed 5 µmol O_2 dm^{-3}. The difference in oxygen content of inflow and outflow water averaged 16.9 µmol dm^{-3} (= 4.7% of air saturation). The mean oxygen consumption was 51.3 µmol O_2 h^{-1} g^{-1} dry weight (calculated $\bar{q}$ = 6.41 mW g^{-1})

suggests an almost exclusively aerobic mechanism sustaining spontaneous activity peaks of *C. abyssorum* under these conditions (Fig. 17), as well as in 10% air saturation (Fig. 11). This in turn was the prerequisite for estimating the likely magnitude of the average lag factor of the respirometer for these periods of observation (Fig. 11).

The effect of varied p_{O_2} on one individual fish embryo (*Salvelinus alpinus*) was investigated with the respirometer-calorimeter (Fig. 18). The eggs of this salmonid species are capable of maintaining a stable level of anoxic heat dissipation over many hours and show a linear dependency of metabolic rate on oxygen up to air saturation as measured with the LKB flow microcalorimeter [13, 16]. After hatching, however, oxygen dependency was only apparent after a sudden fall in p_{O_2}, but within one day the normoxic level of metabolism was reestablished (Fig. 18) (cf. Chap. II.2). Simultaneous direct and indirect calorimetry brings about the resolution of two distinct phases in this acclimatory response to lowered p_{O_2}. (1) Anoxic compensation (24 to 44 h): Here aerobic sources of metabolic energy expenditure (App. C) are augmented by anoxic processes compensating for the drop in metabolic rate as indicated by the increased ratio of measured and calculated heat dissipation. In the calculation the experimentally determined oxycaloric equivalent of aerobic metabolism was used. (2) Conservative (anabolic) compensation (48 to 52 h): Here the ratio of measured

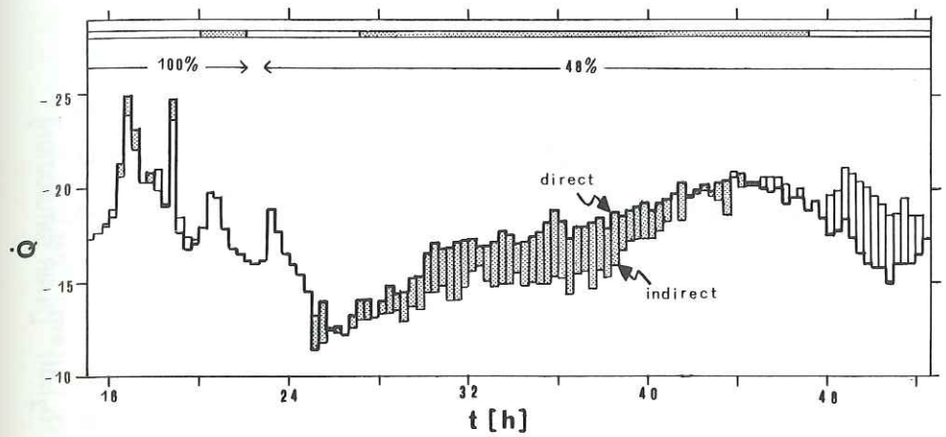

Fig. 18. Simultaneous direct (*thick line*) and indirect (*thin line*) calorimetric measurement of heat dissipation, $\dot{Q}$ [µW], of one individual *Salvelinus alpinus* as a function of externally varied p_{O_2} and time of exposure (at 8°C, constant flow rate of 5.67 cm^3 h^{-1}; 5.11 mg dry weight; see also Figs. 19 and 20). The oxygen consumption under normoxia (p_{O_2} = 19.5 kPA, 0 to 22 h) averaged 157 nmol O_2 h^{-1}. The experimental oxycaloric equivalent averaged −451 kJ (mol O_2)$^{-1}$. After the reduction of oxygen content to 48% air (p_{O_2} = 9.3 kPa) two phases of short-term acclimation became apparent: *anoxic compensation* (25 to 43 h, the *hatched area* indicates the anoxic part of heat dissipation); and *conservative compensation* (44 to 53 h, the *open area* indicates the difference between the expected and observed rate of heat dissipation). The *light* and *dark bar* on the top indicates measuring and calibration positions of the two POS. No estimates of respiratory rates could be obtained during the p_{O_2} transition period (23 to 25 h)

and calculated heat dissipation (App. C) fell below the aerobic value and hence far below the mean ratio for the preceding anoxic compensation period (Fig. 18). This indicates the apparent activation of coupled reactions in which part of the energy that would otherwise be expected to dissipate as heat is conserved. The interesting question arises as to the fate of the accumulated anoxic end product lactic acid [19]. Reutilization in aerobic respiration and coupled glyconeogenesis could theoretically be the explanation [17].

The subsequent test with antibiotics indicated that no bacterial contamination had occurred in this experiment. The animals displayed a highly elevated rate of heat dissipation with large contributions from anoxic sources after exposure to 0.2 g dm^{-3} streptomycin- and neomycinsulfate (Fig. 20, see also Chap. II.9). The simultaneous recorder traces of the calorimeter and respirometer during recovery from this stress are shown in Fig. 19, and the results of the whole experiment are summarized in Fig. 20. It is also interesting to note the similarity of the lag factor of the respirometer calculated for the periods of standard aerobic metabolism and recovery from the drug-induced stress (Fig. 11). For the stress period itself, however, fitting of the respirometer lag factor relative to the *calorimeter* response produces an artifact, as the *physiological* response of the animal is complicated by anoxic processes and cannot be separated from the instrument's response time (Fig. 11).

Contrary to every expectation, further reduction of p_{O_2} to 19% air saturation did not induce a continued activation of anoxic pathways. In fact, as early as 6 h after the

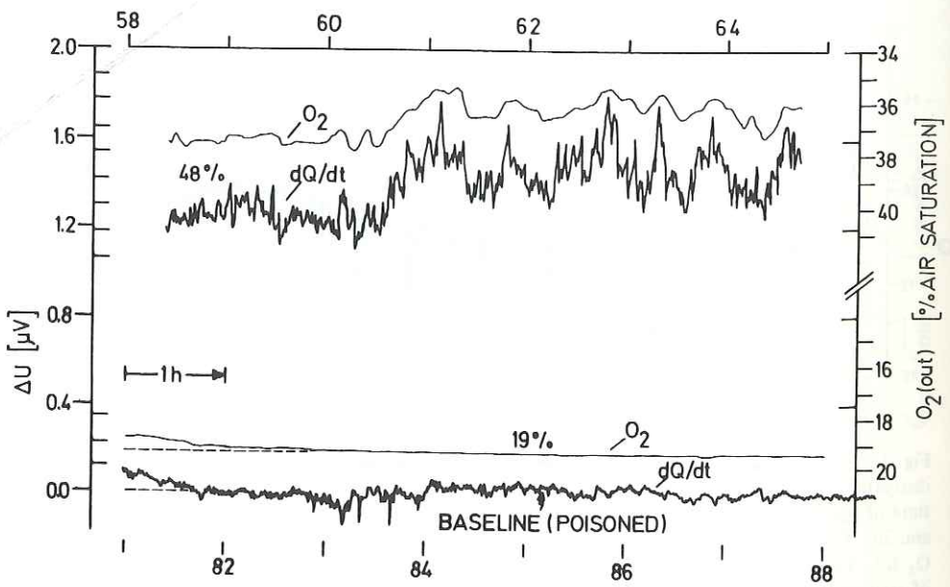

Fig. 19. Recorder traces in a simultaneous calorimetric and respirometric experiment with *Salvelinus alpinus*. A section of the period at 48% air saturation (p_{O_2} = 9.28 kPa) is shown on the top (58 to 65 h). The calorimeter baseline and the outflow oxygen value after poisoning at 19% air saturation of inflow water are shown below (81 to 88 h) (see also Fig. 18)

oxygen transient, a physiological state was observed comparable to the conservative compensation in the above terminology (Fig. 20). The pattern of oxygen consumption leveled off to a rather smooth line, which indicates cessation of locomotory activity and hence a specific reduction of dissipative metabolism under apparently severe hypoxia. Were net-anabolic processes still going on?

Our present understanding of energetic mechanisms involved in coping with variations of the environmental oxygen regime is largely restricted to a descriptive approach in whole animal studies. Oxygen uptake measurements direct interest toward the various expressions of *critical* p_{O_2} [24], without reflecting the most significant metabolic changes that may occur as a result of channeling the energy flow through glycolytic pathways. On the other hand, direct calorimetric results on their own do not provide any information as to the *limiting* p_{O_2} at which anoxic metabolism is switched on to supplement the diminishing aerobic energy source [13, 40]. Besides the aerobic or anoxic *source* of biochemical energy (ATP, electrochemical potentials), external changes in p_{O_2} will also affect the *fate* of this energy: Little is known about the p_{O_2} dependence of *conservative* metabolism, where net-anabolic reactions associated with growth or energy storage reduce the heat change below the value calculated from oxygen consumption using the traditional oxycaloric equivalent (App. C) (Figs. 18, 20). The ratio of observed and expected heat dissipation forms the experimental basis for expressing the "caloric efficiency" [15] and hence quantifying the share of conservative metabolism in the total rate. Again, in invertebrates the rate of *dissipative* metabolism as a function of p_{O_2} [15] has rarely been analyzed in terms of its functional components such as locomotory activity and maintenance (Fig. 14). Direct and indirect calorimetric experiments in open-flow instruments as well as activity measurements and biochemical determinations [19] are required to improve our insight into the regulatory mechanisms underlying the apparently confusing relationship between oxygen conformity and hypoxia tolerance. Not only do studies of the influence of oxygen on animal energetics satisfy the needs of environmental physiologists, but serve equally the exploration of basic principles in cellular physiology.

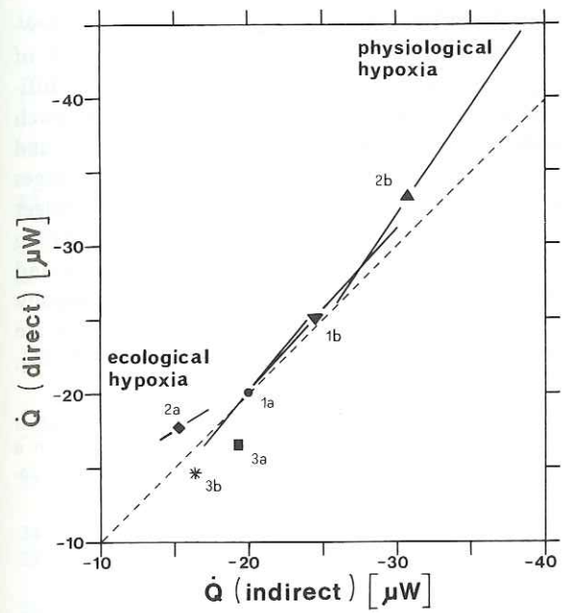

Fig. 20. Relation of direct and indirect calorimetry in *Salvelinus alpinus* during different environmental and physiological conditions. *Hatched line* expected relation on the basis of the theoretical oxycaloric equivalent of −450 kJ $(\text{mol } O_2)^{-1}$. The *symbols* indicate the mean rates during specified periods and the *full lines* are the corresponding regressions (Bartlett's method of best fit) using the lag factors, L_c (see Fig. 11). *1a* normoxic period (see Fig. 18); *2a* anoxic compensation period under *environmental hypoxia* (48% air saturation, see Fig. 18); *2b* anoxic compensation period under *physiological anoxia* (stress period after addition of antibiotics; 48% air saturation). After normalization of the metabolic activity the values returned again to the region of correspondence (*1b*); *3a* conservative compensation period at 48% air saturation (see Fig. 18); *3b* at 19% air saturation after period 1b

The merits of direct calorimetry are on the verge of being recognized in the context of ecophysiological energetics ([13–20, 41], Chap. II.4). In constructing energy budgets we still rely upon our dubious belief in theoretical values for the caloric equivalent of oxygen consumption for most animals, and even these calculations were combined with previously unrecognized errors (App. C).

The contribution of anoxic metabolism during hypoxia and in sustaining high levels of physical activity can be deduced from an increasing bulk of biochemical evidence, while the integrated economy of glycolytic and gluconeogenetic processes and the energetic cost of regulatory mechanisms in anoxic-aerobic transitions can only be

poorly understood without the crucial test by direct and indirect calorimetry. However, most comparative biochemists are reluctant to ponder over the significance of calorimetric and respirometric analyses, and experimental as well as conceptual difficulties of alignment direct such studies into the realm of interdisciplinary research [19]. While progress has been made in the thermochemical analysis of anoxic and aerobic metabolism [15], the possible effect of anabolic processes on the heat changes accompanying aerobic metabolism has not yet even been considered in energy budget calculations for animals. A lesson in microbiology [7], however, suggests elucidating the question of caloric efficiency of animal growth in simultaneous calorimetric and respirometric experiments. Besides tracking the net enthalpy changes that accompany aerobic respiration under various physiological conditions [13, 14], these studies are likely to throw new light on existing theories of biological thermodynamics [6, 15, 36].

Acknowledgments. This work was supported by the *Fonds zur Förderung der wissenschaftlichen Forschung in Österreich,* projects no. 2919 and 3917. Improvements have been achieved in a further development of the twin-flow microrespirometer in cooperation with M. Ortner. This instrument is now commercially available.

References

1. Atkinson HJ, Smith L (1973) An oxygen electrode microrespirometer. J Exp Biol 59:247–253
2. Belaud A, Trotter Y, Peyraud C (1979) Continuous evaluation of $P_{a,02}$ in fish: Recording and data processing. J Exp Biol 82:321–330
3. Bishop J (1976) A continuous recording, differential respirometer for a closed, flowing seawater system. Oikos 27:127–130
4. Brinkhurst RO, Chua KE, Kaushik N (1972) Interspecific interactions and selective feeding by tubificid oligochaetes. Limnol Oceanogr 17:122–133
5. Brkovic-Popovic I, Popovic M (1977) Effects of heavy metals on survival and respiration rate of tubificid worms. II. Effects on respiration rate. Environ Pollut 13:93–98
6. Calow P (1977) Conversion efficiencies in heterotrophic organisms. Biol Rev 52:385–409
7. Dermoun Z, Belaich JP (1979) Microcalorimetric study of *Escherichia coli* aerobic growth: Kinetics and experimental enthalpy associated with growth on succinic acid. J Bacteriol 140: 377–380
8. Dries RR, Eschweiler L, Theede H (1979) An improved equipment for continuous measurement of respiration of marine invertebrates. Kieler Meeresforsch 4:310–316
9. Edwards RW, Learner MA (1960) Some factors affecting the oxygen consumption of *Asellus.* J Exp Biol 37:706–718
10. Evans DO (1972) Correction for lag in continuous-flow respirometry. J Fish Res Board Can 29:1214–1216
11. Fowler JD, Goodnight CJ (1965) The effect of environmental factors on the respiration of *Tubifex.* Am Midl Nat 74:418–428
12. Fry FEJ (1971) The effect of environmental factors on the physiology of fish. In: Hoar WS, Randall DJ (eds) Fish physiology. Academic Press, London New York, pp 1–98
13. Gnaiger E (1979) Direct calorimetry in ecological energetics. Long-term monitoring of aquatic animals. Experientia Suppl 37:155–165
14. Gnaiger E (1980) Energetics of invertebrate anoxibiosis: Direct calorimetry in aquatic oligochaetes. FEBS Lett 112:239–242
15. Gnaiger E (1980) Das kalorische Äquivalent des ATP-Umsatzes im aeroben und anoxischen Metabolismus. Thermochim Acta 40:195–223

16. Gnaiger E (1980) Direct and indirect calorimetry in the study of animal anoxibiosis. A review and the concept of ATP-turnover. In: Hemminger W (ed) Thermal analysis, vol II. ICTA 80. Birkhäuser, Basel Boston Stuttgart, pp 547–552
17. Gnaiger E (1980) The enthalpy of growth – a thermodynamic analysis. Abstr 4th Int Symp Microcalorimetry Appl Biol Univ Coll Wales, Aberystwyth
18. Gnaiger E (1981) Pharmacological application of animal calorimetry. Thermochim Acta 49: 75–85
19. Gnaiger E, Lackner R, Ortner M, Putzer V, Kaufmann R (1981) Physiological and biochemical parameters in anoxic and aerobic energy metabolism of embryonic salmonids, *Salvelinus alpinus.* Eur J Physiol Suppl 391:R57
20. Gnaiger E, Tiefenbrunner F (1982) Microcalorimetry for continuous monitoring of biological processes. In: Message M (ed) Cell and molecular biology in space. Elsevier North Holland, Amsterdam (in press)
21. Gyllenberg G (1973) Comparison of the Cartesian diver technique and the polarographic method, an open system, for measuring the respiratory rates in three marine copepods. Commentat Biol 60:3–13
22. Harnisch P (1935) Versuch einer Analyse des Sauerstoffverbrauchs von *Tubifex tubifex* Müll. Z Vergl Physiol 22:450–465
23. Hart RC (1980) Oxygen consumption in *Caridina nilotica* (Decapoda Atyidae) in relation to temperature and size. Freshwater Biol 10:215–222
24. Herreid CF (1980) Hypoxia in invertebrates. Comp Biochem Physiol 67A:311–320
25. Kamler E (1969) A comparison of the closed-bottle and flowing-water methods for measurement of respiration in aquatic invertebrates. Pol Arch Hydrobiol 16:31–49
26. Kanwisher J (1959) Polarographic oxygen electrode. Limnol Oceanogr 4:210–217
27. Kaufmann R, Gnaiger E (1981) Optimization of calorimetric systems: Continuous control of baseline stability by monitoring thermostat temperatures. Thermochim Acta 49:63–74
28. Kirberger C (1953) Untersuchungen über die Temperaturabhängigkeit von Lebensprozessen bei verschiedenen Wirbellosen. Z Vergl Physiol 35:175–198
29. Klekowski RZ (1971) Cartesian diver microrespirometry for aquatic animals. Pol Arch Hydrobiol 18:93–114
30. Klekowski RZ, Kamler E (1968) Flowing-water polarographic respirometer for aquatic animals. Pol Arch Hydrobiol 15:121–144
31. Koenen ML (1951) Vergleichende Untersuchungen zur Atmungsphysiologie von *Tubifex tubifex* M. und *Limnodrilus claparedeanus* R. Z Vergl Physiol 33:436–456
32. Lasserre P, Renaud-Mornant J (1973) Resistance and respiratory physiology of intertidal meiofauna to oxygen-deficiency. Neth J Sea Res 7:290–302
33. Lovtrup S (1973) The construction of a microrespirometer for the determination of respiratory rates of eggs and small embryos. In: Kerkut G (ed) Experiments in physiology and biochemistry, vol VI. Academic Press, London New York, pp 115–152
34. Mangum C, Winkle Van W (1973) Responses of aquatic invertebrates to declining oxygen conditions. Am Zool 13:529–541
35. Milsum JH (1966) Biological control systems analysis. McGraw-Hill Electronic Science Series, New York, 466 pp
36. Morowitz HJ (1978) Energy flow in biology. Academic Press, London New York, 344 pp
37. Nagell B (1975) The open-flow respirometric method: precision of measurement in general and description of a high precision respirometer for aquatic animals. Int Rev Gesamten Hydrobiol 60:655–667
38. Nimi AJ (1978) Lag adjustment between estimated and actual physiological responses conducted in flow-through systems. J Fish Res Board Can 35:1265–1269
39. Olson TA, Rueger ME, Scofield JI (1969) Flow-through polarographic respirometry for aquatic animals. Hydrobiologia 34:322–329
40. Palmer MF (1970) Aspects of the respiratory physiology of *Tubifex tubifex* in relation to its ecology. Zool London 154:463–473
41. Pamatmat MM (1978) Oxygen uptake and heat production in a metabolic conformer (*Littorina irrorata*) and a metabolic regulator (*Uca pugnax*). Mar Biol 48:317–325

42. Pattee E (1965) Sténothermie et eurythermie les invertébrés d'eau douce et la variation journaliére de tempépature. Ann Limnol 1:281–434
43. Platzer I (1967) Untersuchungen zur Temperaturadaptation der tropischen Chironomidenart *Chironomus strenskei* Fittkau (Diptera). Z Vergl Physiol 54:58–74
44. Richman S (1958) The transformation of energy by *Daphnia pulex*. Ecol Monogr 28:273–291
45. Rohde RA (1960) The influence of carbon dioxide on respiration of certain plant-parasitic nematodes. Proc Helminthol Soc Wash 27:160–164
46. Spink C, Wadsö I (1976) Calorimetry as an analytical tool in biochemistry and biology. In: Glick D (ed) Methods in biochemical analysis, vol 23. Wiley-Science, New York, pp 1–159
47. Whitley LS, Sikora RA (1970) The effect of 3 common pollutants on the respiration rate of tubificid worms. J Water Pollut Contrib Fed 42:R57–R66
48. Wightman JA (1977) Respirometry techniques for terrestrial invertebrates and their application to energetics studies. NZJ Zool 4:453–469
49. Zeuthen E (1950) Cartesian diver respirometer. Biol Bull 98:303–318